Charge-Noise-Induced Dephasing in Silicon Hole-Spin Qubits

Ognjen Malkoc,[1] Peter Stano,[1,2,*] and Daniel Loss[1,3,4]
[1]RIKEN Center for Emergent Matter Science, Wako-shi, Saitama 351-0198, Japan
[2]Institute of Physics, Slovak Academy of Sciences, 845 11 Bratislava, Slovakia
[3]RIKEN Center for Quantum Computing, Wako, Saitama 351-0198, Japan
[4]Department of Physics, University of Basel, Klingelbergstrasse 82, CH-4056 Basel, Switzerland

(Received 23 January 2022; revised 27 September 2022; accepted 9 November 2022; published 8 December 2022)

We investigate, theoretically, charge-noise-induced spin dephasing of a hole confined in a quasi-two-dimensional silicon quantum dot. Central to our treatment is accounting for higher-order corrections to the Luttinger Hamiltonian. Using experimentally reported parameters, we find that the new terms give rise to sweet spots for the hole-spin dephasing, which are sensitive to device details: dot size and asymmetry, growth direction, and applied magnetic and electric fields. Furthermore, we estimate that the dephasing time at the sweet spots is boosted by several orders of magnitude, up to on the order of milliseconds.

DOI: 10.1103/PhysRevLett.129.247701

Introduction.—Silicon is promising for realizing scalable qubits using quantum-dot electrons to store and process quantum information [1–4]. The recent attention to silicon stems from compatibility with industrial fabrication [5–7] and low noise from nuclear spins. The latter effect, so far a major obstacle for spin qubits in GaAs, can be further suppressed using holes instead of electrons [8–11]. Holes also offer stronger spin-orbit coupling [12–15], essential for electric spin control without micromagnets or on-chip ESR lines [16]. Taken together, the reduced susceptibility to nuclear noise [17], the absence of valley degeneracy, and fully electric control, make holes in silicon an attractive platform for scalable spin qubits.

In a quasi-two-dimensional quantum dot with the strongest confinement along the growth direction (a lateral dot), the confinement splits the bulk fourfold degeneracy at the Γ point into light and heavy holes, offering a resilient spin qubit residing in the heavy hole subspace [8,18,19]. Spin blockade detection [20–23], control over the charge state down to a single hole [24,25], fabrication of arrays [26–28], and demonstration of single [29,30] and two-qubit operations [31] are among recent experimental achievements with lateral dots. In contrast, the strong confinement-induced spin-orbital mixing in a nanowire geometry [32–34] gives large and tunable spin-orbit interaction [35–38] and fast spin manipulation [39,40].

The strong sensitivity to the electric field is a generic feature of hole-spin qubits. Among its most direct manifestations, the electrical response of the g factor has been reported for various designs [33,41–50]. While it offers increased electrical tunability, it also implies a higher susceptibility to electrical noise. With nuclear noise suppressed, charge noise becomes the primary concern for qubit coherence [16,51,52]. Aiming at long coherence time, the most favorable scenario seems to be a single hole in an isolated lateral quantum dot. Assessing this ultimate limit on the hole-spin coherence is our main objective.

We find that in lateral dots the spin-electric coupling is dominated by higher-order (nonquadratic in momentum) terms, which are not contained in the often used and well-known Luttinger Hamiltonian [53]. This finding is among our main results.

While the conduction band nonparabolicity has been studied in zinc-blende crystals in detail [54,55], including its effects on the g factor [56], the valence band requires a separate treatment. To this end, we derive the corrections to the Luttinger Hamiltonian up to the fourth order in momentum and up to linear in the electric field. Even though one can generate these terms by symmetry analysis, for example using the tables in Ref. [57], we are not aware of their prefactors being known. To evaluate the spin-orbit effects reliably, these prefactors are necessary. We calculate them within the 14-band $k \cdot p$ model [58], using up to the fifth-order Löwdin perturbation theory. The resulting effective model is valid for any materials with diamond crystal structures, such as Si and Ge, but we focus on the former material.

We obtain the spin-qubit Hamiltonian by projecting the valence band Hamiltonian onto the lowest orbital state defined by the three-dimensional confinement. We use second-order perturbation theory to include the effects of higher orbital states. From the qubit Hamiltonian we evaluate two quantities of interest: the g tensor and the dephasing rate. Our main result in this part is twofold. First, we find a typical dephasing time on the order of tens of microseconds. This value is then the ultimate upper limit in any design with holes in silicon gated dots with an in-plane magnetic field. With other than lateral dots one would expect the dephasing time to be much smaller. Second, we find pronounced sweet spots, where the dephasing time is boosted up to milliseconds. Their position in parameter space is sensitive to all system parameters. The suggestion to search for experimentally robust sweet spots is the main practical implication of our Letter.

Valence band corrections.—All symmetry-allowed terms in the silicon valence band up to quadratic in the kinetic momentum $\hbar\mathbf{k}$ are contained in the Luttinger Hamiltonian [53],

$$H_L = \frac{\hbar^2}{2m_0}\left[-\left(\gamma_1 + \frac{5\gamma_2}{2}\right)k^2 + 2\gamma_2(k_X^2 J_X^2 + k_Y^2 J_Y^2 + k_Z^2 J_Z^2) + 4\gamma_3(k_{XY}J_{XY} + k_{YZ}J_{YZ} + k_{ZX}J_{ZX})\right] - 2\mu_B(\kappa\mathbf{J} + q\mathbf{J}_3)\cdot\mathbf{B}. \quad (1)$$

Here, X, Y, and Z denote the [100], [010], and [001] crystallographic axis, respectively, $\mathbf{B}$ is the magnetic field entering the momentum $\hbar\mathbf{k} = -i\hbar\nabla + e\mathbf{A}$ via the vector potential $\mathbf{A}$, the components of the vectors $\mathbf{J} = (J_X, J_Y, J_Z)$ and $\mathbf{J}_3 = (J_X^3, J_Y^3, J_Z^3)$ are the spin 3/2 operators, m_0 is the free-electron mass, $C_{ij} = C_iC_j + C_jC_i$ is the anticommutator, and the coefficients $\gamma_1, \gamma_2, \gamma_3, \kappa$, and q are the Luttinger parameters [59].

Using symmetry analysis, we derive corrections to Eq. (1) up to the fourth order in momentum getting fifteen terms [60]. We evaluate their prefactors using the 14-band $k\cdot p$ model in the fourth order of the Löwdin perturbation theory [61]. With the full list including formulas for prefactors given elsewhere, we restrict here ourselves to an excerpt. Based on the analysis outlined below, we identify terms contributing dominantly to spin dephasing for devices grown along [001] [62]. There are magnetic-field generated terms,

$$\begin{aligned} H_{41} &= \mu_B(\kappa_{41}\mathbf{J} + q_{41}\mathbf{J}_3)\cdot\mathbf{B}(k_X^2 + k_Y^2 + k_Z^2),\\ H_{42} &= \mu_B(\kappa_{42}\mathbf{J} + q_{42}\mathbf{J}_3)\cdot(B_Xk_X^2, B_Yk_Y^2, B_Zk_Z^2),\\ H_{43} &= \mu_B(\kappa_{43}\mathbf{J} + q_{43}\mathbf{J}_3)\cdot[k_X(k_YB_Y + k_ZB_Z), \text{c.p.}],\\ H_{53} &= \mu_B\Gamma_{53}\mathbf{J}_{53}\cdot[B_X(k_Y^2 - k_Z^2), \text{c.p.}], \end{aligned} \quad (2a)$$

and the band-warping terms,

$$\begin{aligned} H_{12} &= \Gamma_{12}(\{k_X, k_Y\}^2 + \{k_Y, k_Z\}^2 + \{k_Z, k_X\}^2),\\ H_{32} &= \Gamma_{32}\mathbf{J}_{32}\cdot(2k_X^2k_Y^2 - (k_Y^2 + k_X^2)k_Z^2, (k_Y^2 - k_X^2)k_Z^2). \end{aligned} \quad (2b)$$

In these equations, $\mathbf{J}_{53} = (\{J_x, J_y^2 - J_z^2\}, \{J_y, J_z^2 - J_x^2\}, \{J_z, J_x^2 - J_y^2\})$, $\mathbf{J}_{32} = (J_Z^2 - \mathbf{J}\cdot\mathbf{J}/3, J_X^2 - J_Y^2)$, and c.p. means cyclic permutation. The prefactor values are given in Table I of the Supplemental Material [63]. The figures in the following sections are plotted using all 15 corrections, together denoted as δH_L. In the Supplemental Material [63], we show analogous figures produced with Eq. (2) showing good correspondence.

Effective hole-spin qubit Hamiltonian.—We consider a hole confined in a device shown in Fig. 1(a). We denote the hole-spin subspace by index J, with $J = |J_z| \in \{1/2, 3/2\}$ for the light and heavy hole, respectively. The two

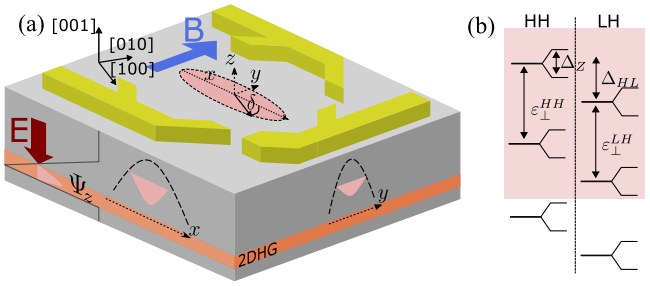

FIG. 1. (a) Lateral quantum dot hosting a spin qubit. A hole is confined by a triangular potential along the growth direction z, and an in-plane harmonic potential with axes x and y rotated by δ with respect to the crystallographic directions [100] and [010]. (b) The basis states in the calculation, showing the heavy hole and light hole subbands of the unperturbed Hamiltonian. The red area shows the states used in the perturbation series of Eq. (6).

subspaces are split in energy by the heavy-hole–light-hole splitting Δ_{HL} which depends on the growth direction and strain [65–68,70–72] (see Supplemental Material Appendix D for a short discussion). We assume that the heavy hole subspace is the ground state and the qubit is defined therein, as a configuration most resilient to charge noise. The masses of holes are anisotropic and spin dependent and we use $m_{J,xy}$ for the spin-J in-plane mass and $m_{J,z}$ for the mass along z. Expressions for masses in terms of the Luttinger parameters are given in the Supplemental Material Table II.

We adopt standard choices to describe the quantum dot confinement: a triangular potential for the vertical part and an anisotropic harmonic for the in-plane part,

$$V_{xy} = \frac{m_{3/2,xy}}{2\hbar^2}(\varepsilon_x^2x^2 + \varepsilon_y^2y^2), \qquad V_z = \begin{cases} eE_zz & \text{for } z > 0\\ V_0 & \text{for } z \le 0 \end{cases}. \quad (3)$$

Here, V_0 is the heterostructure band offset, ε_x and ε_y are the in-plane excitation energies, E_z is the electric field, and x, y, and z are dot coordinates. In calculations, we take the limit $V_0 \to \infty$, resulting in a vanishing wave function for $z \le 0$ [76]. Having specified the confinement, we have

$$H = H_L + \delta H_L - V_{xy} - V_z, \quad (4)$$

as the full—three-dimensional—Hamiltonian describing the confined hole. Next, we reduce this microscopic description into an effective Hamiltonian for the spin qubit, a two-level system.

We first define the unperturbed Hamiltonian by supplementing the confinement by terms quadratic in momentum and not coupling the heavy-hole and light-hole subspaces,

$$H_0^J = \frac{\hbar^2(\partial_x^2 + \partial_y^2)}{2m_{J,xy}} + \frac{\hbar^2\partial_z^2}{2m_{J,z}} - V_{xy} - V_z. \quad (5)$$

The unperturbed Hamiltonian defines the basis for the perturbation theory. Since it is separable in in-plane coordinates x and y, the vertical coordinate z, and the spin, the basis states $|J, n_x, n_y, n_z\rangle$ can be indexed by four quantum numbers: the pair (n_x, n_y) is the Fock-Darwin spectrum indexes, while n_z labels eigenstates of the triangular potential, associated with energy scale $(\hbar e E_z/\sqrt{m_{J,z}})^{2/3}$ (see Appendix A1 in Ref. [79] for details on triangular-confinement eigenstates). The splitting of heavy and light holes Δ_{HL} is the energy difference of the two ground states of Eq. (5) for the two values of the spin index J.

The qubit Hamiltonian follows by integrating out the orbital degrees of freedom, with the excited states taken into account within the second-order perturbation theory,

$$\mathcal{H} = \langle J, \mathbf{0}| \left[H + \sum_{(J',\mathbf{n})\neq(J,\mathbf{0})} \frac{\delta H |J', \mathbf{n}\rangle\langle J', \mathbf{n}| \delta H}{E_{|J,\mathbf{0}\rangle} - E_{|J',\mathbf{n}\rangle}} \right] |J, \mathbf{0}\rangle. \quad (6)$$

Here, $\delta H = H - H_0^J$, the summation is over all excited orbital states, the vector $\mathbf{n} = (n_x, n_y, n_z)$, and $E_{|J,\mathbf{n}\rangle}$ is the unperturbed eigenstate energy.

This derivation follows the procedure of Refs. [56,79] with one difference. In those references, the reduction proceeded in two steps: first integrating out the vertical coordinate z, then the in-plane coordinates x and y. Here we include in-plane excitation energies in the denominator of Eq. (6), as they are comparable to Δ_{HL}. Considering quasi-two-dimensional dots, we restrict the sum over n_z in Eq. (6) to the lowest excited state [see Fig. 1(b)]. The resulting approximate form of $\mathcal{H}$ is the basis for the two main quantities of our Letter, the effective g tensor, and the qubit energy. The dependence of the latter on the electric field is responsible for dephasing of the hole-spin qubit.

Effective g tensor.—Evaluating Eq. (6) gives the Hamiltonian $\mathcal{H}$ describing the qubit as a two-level system. Because of time-reversal symmetry, at zero magnetic field the two states are degenerate. Considering only linear magnetic field terms, an approximation that we adopt in evaluating Eq. (6), we obtain the Hamiltonian of a spin one-half,

$$\mathcal{H} = \sum_{i,j=x,y,z} \mu_B B_i \hat{g}_{ij} \tau_j. \quad (7)$$

Here, $\boldsymbol{\tau}$ is a vector of Pauli matrices defined with up and down spin one-half states corresponding to perturbed spin states, where the perturbation in Eq. (6) admixes the light-hole states to the heavy-hole ground state, and $\hat{g}$ is a second-rank tensor, the g tensor. We have thus reduced the three-dimensional qubit description of Eq. (4) to a simpler effective two-level model. Nevertheless, this model reflects orbital effects through the g-tensor dependence on confinement electric fields, which we now examine.

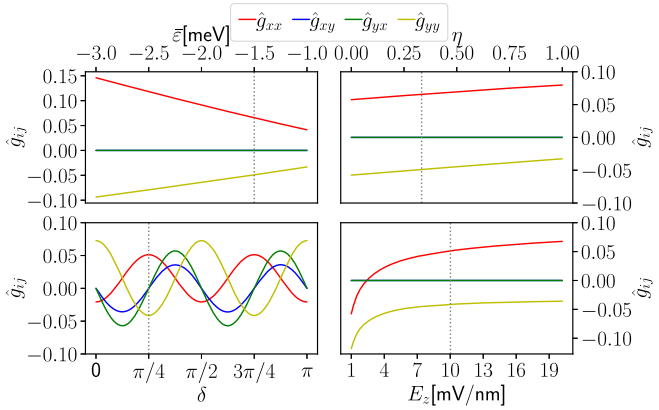

FIG. 2. Heavy-hole qubit g-tensor components for a dot with z axis along [001]. The horizontal axis represents (a) the average dot energy $\bar{\varepsilon} = (\varepsilon_x + \varepsilon_y)/2$, (b) dot asymmetry $\eta = (\varepsilon_y - \varepsilon_x)/2\bar{\varepsilon}$, (c) dot orientation δ, and (d) vertical confinement electric field E_z. The dashed line, defined by $\varepsilon_x = -1$ meV, $\varepsilon_y = -3$ meV, $\delta = \pi/4$, and $E_z = 10$ mV/nm, denotes a common reference point.

Figure 2 shows the g tensor for a [001]-grown quantum dot. The g tensor in-plane components are plotted as functions of the dot in-plane size [panel (a)], asymmetry [panel (b)], orientation [panel (c)], and the vertical-confinement strength [panel (d)]. The off-diagonal components g_{xz}, g_{zx}, g_{yz}, and g_{zy}, are zero. The out-of-plane component g_{zz} is typically an order of magnitude larger than the in-plane ones, and does not depend appreciably on any parameter except of the vertical electric field. We include g_{zz} in Fig. S2 of the Supplemental Material. The g tensor is strongly anisotropic, a consequence of the confinement breaking all crystal symmetries [80,81]. In realistic samples, which are neither perfectly symmetric nor aligned with any particular direction with respect to the crystal axes, one expects large variations of the g-tensor components. Most importantly, the g-tensor components clearly depend on the confinement electric field.

Coherence time.—The charge noise in the sample and experiment electronics leads to fluctuations of the electric field at the dot location, and thereby to fluctuations of the qubit energy through changes of the g tensor. The electric field enters the g tensor in two ways: by defining the shape of the dot confinement and by inducing band-structure terms. We find that the latter are negligible [82]. We also neglect fluctuating electric in-plane fields, since a uniform field does not change the shape of a harmonic confinement adopted in our model. The noise in the z component of the electric field remains, changing the qubit energy through changes in the vertical confinement strength. The noise is described by its spectrum, $S(f) = \int_{-\infty}^{\infty} d\tau e^{i2\pi f\tau} \langle E_z(0) E_z(\tau)\rangle$, with the bracket standing for statistical average. We further assume that $1/f$ noise is dominant and take $S(f) = A/|f|$ [83].

Reference [75] finds that $1/f$ noise causes a Gaussian decay with a pure-dephasing rate

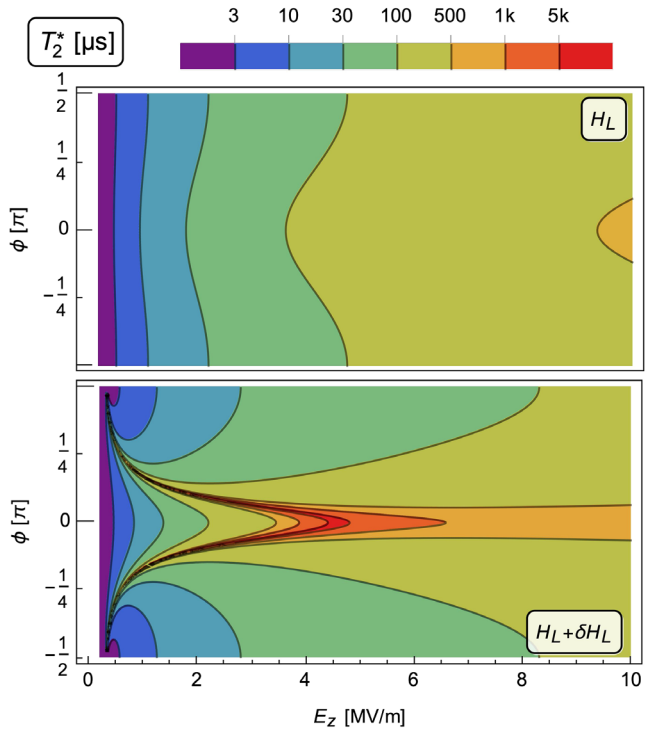

FIG. 3. Dephasing time T_2^* calculated from the Luttinger model (top) and the full Hamiltonian (bottom). Figure axes: the vertical electric field E_z and the in-plane-direction angle ϕ of the magnetic field $\mathbf{B} = B(\cos\phi, \sin\phi, 0)$. Other parameters: $B = 1$ T, confinement lengths $l_x = \hbar\sqrt{(\gamma_1+\gamma_2)/m_0\varepsilon_x} = 20$ nm, $l_y = 15$ nm, the dot-orientation angle $\delta = 0$, the noise magnitude $A = 450$ V^2/m^2 [73,74], and the frequency cutoffs $f_{\mathrm{ir}} = 1$ Hz, $t = 10$ μs.

$$1/T_2^* = |\partial_{E_z}\omega|\sqrt{A\ln(1/2\pi f_{\mathrm{ir}}t)}, \tag{8}$$

where f_{ir} is the low-frequency cutoff, t is a time of order of the dephasing time T_2^*, and $\hbar\omega$ is the qubit energy. We evaluate it using Eq. (7) as $\hbar\omega = \sqrt{\mu_B^2 B_j B_k g_{ji} g_{ki}}$, summing over repeated indexes.

Our main result is the analysis of the dephasing time T_2^* calculated from Eq. (8). The upper panel of Fig. 3 shows T_2^* calculated using the Luttinger model. The lower panel shows the results upon adding the fourth-order terms δH_L. The dephasing time ranges from tens to hundreds of μs in most of the plot area. In both models, at large electric fields, the dephasing time is maximized for the B field along a crystallographic axis. However, including δH_L reveals a line of sweet spots with the dephasing time boosted beyond a millisecond. We have examined other configurations and found similar behavior [85]. We thus conclude that, on the one hand, one might suspect qualitative discrepancies between the Luttinger model and its next-order extension, and on the other, that sweet spots in lateral spin hole qubits are generic [15,40].

Taken from a broader perspective, the above discrepancy suggests a generic issue with the analysis of hole-spin qubits based solely on the Luttinger model. It is due to distinct dispersion terms arising only beyond the third-order of $k\cdot p$ perturbation theory, namely, "spin-orbit" terms which are not time-reversal symmetric [86]. We suspect that some existing analytical results on the hole g factor and related quantities might be affected. On the other hand, results based on exact diagonalization of multiband $k\cdot p$ Hamiltonians—if including enough bands—are not affected since they effectively contain all perturbation orders, including the fourth. Finally, concerning fitting experimental data by theory models, large uncertainty in the input parameters (especially strain and confinement details) might influence results as much or even more than including or not including the fourth-order terms in the dispersion.

Before concluding, we review available experimental results on the confined hole spin dephasing times. There are not many: An optical probe of a single hole in a III-V self-assembled dot gave T_2^* of 100 ns in Ref. [87] and 0.5 μs in Ref. [11], with the coherence time T_2 estimated an order of magnitude larger. The only numbers we are aware of in silicon is $T_2^* = 60$ ns from Ref. [16], which was prolonged fourfold upon Hahn-echo, as expected for a $1/f$ noise [88], and $T_2^* = 440$ ns from Ref. [14] for a hole spin qubit in a Si FinFET device.

While all these numbers are lower than our T_2^*, the difference is not so drastic considering that the charge noise levels have large variations among different materials and samples [74,89]. Coincidentally, the dephasing times that we obtained are comparable to nuclear-limited dephasing times of electrons in silicon dots: T_2^* in natural silicon is a few microseconds, close to our values away from the sweet spot, and a millisecond in purified silicon-28, comparable to our sweet-spot values. We conclude that the intrinsic charge noise might be limiting coherence in some of these experiments, while in others, such as Si FinFETs, the nuclear noise is still the limiting factor, see Refs. [14,17]. Our results suggest that holes in lateral dots can reach coherence comparable to electrons [90], and searching for the hole-qubit sweet spots experimentally looks attractive.

Conclusions.—In this Letter, we have quantified the g tensor and the charge-noise-induced dephasing of a silicon spin hole qubit. For typical dot dimensions and external magnetic and electric fields, we find it is necessary to go beyond the Luttinger model to assess the g tensor and dephasing reliably; the difference is qualitative. Our model, which can also be extended to devices using other diamond crystal materials, for example germanium, predicts sweet spots for the dephasing time. We find that the sweet spots depend on the device growth direction, confinement potential, and in-plane magnetic field orientation. Our Letter leaves space for interesting extensions. For example, the dependence on the device geometry prompts the question

of how the additional spin-orbit interactions impact spin dephasing in other devices, such as nanowire-based hole-spin qubits [36] or FinFETs [15].

We thank Ch.-H. Hsu for useful discussions. We acknowledge the financial support from CREST JST (JPMJCR1675), the Swiss National Science Foundation, and NCCR SPIN (Grant No. 51NF40-180604).

Note added.—Recently, Ref. [93] reported experimental detection of sweet spots in a single-hole Si-finFET device. The dephasing time T_2^* (T_2^{Hahn}) reached 6 μs (88 μs) and showed variation by a factor of almost 3 (more than 4) upon changing the magnetic field direction.

*Corresponding author.
peter.stano@riken.jp

[1] D. Loss and D. P. DiVincenzo, Phys. Rev. A **57**, 120 (1998).
[2] A. Chatterjee, P. Stevenson, S. De Franceschi, A. Morello, N. P. de Leon, and F. Kuemmeth, Nat. Rev. Phys. **3**, 157 (2021).
[3] P. Stano and D. Loss, Nat. Rev. Phys. **4**, 672 (2022).
[4] G. Burkard, T. D. Ladd, J. M. Nichol, A. Pan, and J. R. Petta, arXiv:2112.08863.
[5] S. Thompson, Guangyu Sun, Youn Sung Choi, and T. Nishida, IEEE Trans. Electron Devices **53**, 1010 (2006).
[6] M. F. Gonzalez-Zalba, S. de Franceschi, E. Charbon, T. Meunier, M. Vinet, and A. S. Dzurak, National electronics review **4**, 872 (2021).
[7] A. M. J. Zwerver *et al.*, National electronics review **5**, 184 (2022).
[8] D. V. Bulaev and D. Loss, Phys. Rev. Lett. **95**, 076805 (2005).
[9] D. Heiss, S. Schaeck, H. Huebl, M. Bichler, G. Abstreiter, J. J. Finley, D. V. Bulaev, and D. Loss, Phys. Rev. B **76**, 241306(R) (2007).
[10] E. A. Chekhovich, A. B. Krysa, M. S. Skolnick, and A. I. Tartakovskii, Phys. Rev. Lett. **106**, 027402 (2011).
[11] J. H. Prechtel, A. V. Kuhlmann, J. Houel, A. Ludwig, S. R. Valentin, A. D. Wieck, and R. J. Warburton, Nat. Mater. **15**, 981 (2016).
[12] A. Bogan, S. Studenikin, M. Korkusinski, L. Gaudreau, P. Zawadzki, A. S. Sachrajda, L. Tracy, J. Reno, and T. Hargett, Phys. Rev. Lett. **120**, 207701 (2018).
[13] B. Venitucci and Y.-M. Niquet, Phys. Rev. B **99**, 115317 (2019).
[14] L. C. Camenzind, S. Geyer, A. Fuhrer, R. J. Warburton, D. M. Zumbühl, and A. V. Kuhlmann, National electronics review **5**, 178 (2022).
[15] S. Bosco, B. Hetényi, and D. Loss, PRX Quantum **2**, 010348 (2021).
[16] R. Maurand, X. Jehl, D. Kotekar-Patil, A. Corna, H. Bohuslavskyi, R. Laviéville, L. Hutin, S. Barraud, M. Vinet, M. Sanquer, and S. De Franceschi, Nat. Commun. **7**, 13575 (2016).
[17] S. Bosco and D. Loss, Phys. Rev. Lett. **127**, 190501 (2021).
[18] D. V. Bulaev and D. Loss, Phys. Rev. Lett. **98**, 097202 (2007).
[19] R. W. Martin, R. J. Nicholas, G. J. Rees, S. K. Haywood, N. J. Mason, and P. J. Walker, Phys. Rev. B **42**, 9237 (1990).
[20] R. Li, F. E. Hudson, A. S. Dzurak, and A. R. Hamilton, Nano Lett. **15**, 7314 (2015).
[21] H. Bohuslavskyi, D. Kotekar-Patil, R. Maurand, A. Corna, S. Barraud, L. Bourdet, L. Hutin, Y.-M. Niquet, X. Jehl, S. De Franceschi, M. Vinet, and M. Sanquer, Appl. Phys. Lett. **109**, 193101 (2016).
[22] Y. Yamaoka, K. Iwasaki, S. Oda, and T. Kodera, Jpn. J. Appl. Phys. **56**, 04CK07 (2017).
[23] D. Q. Wang, O. Klochan, J.-T. Hung, D. Culcer, I. Farrer, D. A. Ritchie, and A. R. Hamilton, Nano Lett. **16**, 7685 (2016).
[24] S. D. Liles, R. Li, C. H. Yang, F. E. Hudson, M. Veldhorst, A. S. Dzurak, and A. R. Hamilton, Nat. Commun. **9**, 3255 (2018).
[25] A. J. Sousa de Almeida, A. M. Seco, T. van den Berg, B. van de Ven, F. Bruijnes, S. V. Amitonov, and F. A. Zwanenburg, Phys. Rev. B **101**, 201301(R) (2020).
[26] N. W. Hendrickx, W. I. L. Lawrie, M. Russ, F. van Riggelen, S. L. de Snoo, R. N. Schouten, A. Sammak, G. Scappucci, and M. Veldhorst, Nature (London) **591**, 580 (2021).
[27] W. I. L. Lawrie, H. G. J. Eenink, N. W. Hendrickx, J. M. Boter, L. Petit, S. V. Amitonov, M. Lodari, B. Paquelet Wuetz, C. Volk, S. G. J. Philips, G. Droulers, N. Kalhor, F. van Riggelen, D. Brousse, A. Sammak, L. M. K. Vandersypen, G. Scappucci, and M. Veldhorst, Appl. Phys. Lett. **116**, 080501 (2020).
[28] F. van Riggelen, N. W. Hendrickx, W. I. L. Lawrie, M. Russ, A. Sammak, G. Scappucci, and M. Veldhorst, Appl. Phys. Lett. **118**, 044002 (2021).
[29] D. Jirovec, A. Hofmann, A. Ballabio, P. M. Mutter, G. Tavani, M. Botifoll, A. Crippa, J. Kukucka, O. Sagi, F. Martins, J. Saez-Mollejo, I. Prieto, M. Borovkov, J. Arbiol, D. Chrastina, G. Isella, and G. Katsaros, Nat. Mater. **20**, 1106 (2021).
[30] N. W. Hendrickx, W. I. L. Lawrie, L. Petit, A. Sammak, G. Scappucci, and M. Veldhorst, Nat. Commun. **11**, 3478 (2020).
[31] N. W. Hendrickx, D. P. Franke, A. Sammak, G. Scappucci, and M. Veldhorst, Nature (London) **577**, 487 (2020).
[32] Y. Hu, F. Kuemmeth, C. M. Lieber, and C. M. Marcus, Nat. Nanotechnol. **7**, 47 (2012).
[33] V. S. Pribiag, S. Nadj-Perge, S. M. Frolov, J. W. G. van den Berg, I. van Weperen, S. R. Plissard, E. P. A. M. Bakkers, and L. P. Kouwenhoven, Nat. Nanotechnol. **8**, 170 (2013).
[34] F. Gao, J.-H. Wang, H. Watzinger, H. Hu, M. J. Rančić, J.-Y. Zhang, T. Wang, Y. Yao, G.-L. Wang, J. Kukučka, L. Vukušić, C. Kloeffel, D. Loss, F. Liu, G. Katsaros, and J.-J. Zhang, Adv. Mater. **32**, 1906523 (2020).
[35] C. Kloeffel, M. Trif, and D. Loss, Phys. Rev. B **84**, 195314 (2011).
[36] F. N. M. Froning, M. J. Rančić, B. Hetényi, S. Bosco, M. K. Rehmann, A. Li, E. P. A. M. Bakkers, F. A. Zwanenburg, D. Loss, D. M. Zumbühl, and F. R. Braakman, Phys. Rev. Res. **3**, 013081 (2021).
[37] C. Kloeffel, M. J. Rančić, and D. Loss, Phys. Rev. B **97**, 235422 (2018).

[38] S. Bosco, M. Benito, C. Adelsberger, and D. Loss, Phys. Rev. B **104**, 115425 (2021).
[39] F. N. M. Froning, L. C. Camenzind, O. A. H. van der Molen, A. Li, E. P. A. M. Bakkers, D. M. Zumbühl, and F. R. Braakman, Nat. Nanotechnol. **16**, 308 (2021).
[40] Z. Wang, E. Marcellina, A. R. Hamilton, J. H. Cullen, S. Rogge, J. Salfi, and D. Culcer, npj Quantum Inf. **7**, 54 (2021).
[41] T. Andlauer and P. Vogl, Phys. Rev. B **79**, 045307 (2009).
[42] G. Katsaros, P. Spathis, M. Stoffel, F. Fournel, M. Mongillo, V. Bouchiat, F. Lefloch, A. Rastelli, O. G. Schmidt, and S. De Franceschi, Nat. Nanotechnol. **5**, 458 (2010).
[43] F. Klotz, V. Jovanov, J. Kierig, E. C. Clark, D. Rudolph, D. Heiss, M. Bichler, G. Abstreiter, M. S. Brandt, and J. J. Finley, Appl. Phys. Lett. **96**, 053113 (2010).
[44] N. Ares, V. N. Golovach, G. Katsaros, M. Stoffel, F. Fournel, L. I. Glazman, O. G. Schmidt, and S. De Franceschi, Phys. Rev. Lett. **110**, 046602 (2013).
[45] A. J. Bennett, M. A. Pooley, Y. Cao, N. Sköld, I. Farrer, D. A. Ritchie, and A. J. Shields, Nat. Commun. **4**, 1522 (2013).
[46] J. H. Prechtel, F. Maier, J. Houel, A. V. Kuhlmann, A. Ludwig, A. D. Wieck, D. Loss, and R. J. Warburton, Phys. Rev. B **91**, 165304 (2015).
[47] M. Brauns, J. Ridderbos, A. Li, E. P. A. M. Bakkers, and F. A. Zwanenburg, Phys. Rev. B **93**, 121408 (2016).
[48] B. Voisin, R. Maurand, S. Barraud, M. Vinet, X. Jehl, M. Sanquer, J. Renard, and S. De Franceschi, Nano Lett. **16**, 88 (2016).
[49] F. K. de Vries, J. Shen, R. J. Skolasinski, M. P. Nowak, D. Varjas, L. Wang, M. Wimmer, J. Ridderbos, F. A. Zwanenburg, A. Li, S. Koelling, M. A. Verheijen, E. P. A. M. Bakkers, and L. P. Kouwenhoven, Nano Lett. **18**, 6483 (2018).
[50] A. Crippa, R. Maurand, L. Bourdet, D. Kotekar-Patil, A. Amisse, X. Jehl, M. Sanquer, R. Laviéville, H. Bohuslavskyi, L. Hutin, S. Barraud, M. Vinet, Y.-M. Niquet, and S. De Franceschi, Phys. Rev. Lett. **120**, 137702 (2018).
[51] J. Houel, J. H. Prechtel, A. V. Kuhlmann, D. Brunner, C. E. Kuklewicz, B. D. Gerardot, N. G. Stoltz, P. M. Petroff, and R. J. Warburton, Phys. Rev. Lett. **112**, 107401 (2014).
[52] J. Yoneda, K. Takeda, T. Otsuka, T. Nakajima, M. R. Delbecq, G. Allison, T. Honda, T. Kodera, S. Oda, Y. Hoshi, N. Usami, K. M. Itoh, and S. Tarucha, Nat. Nanotechnol. **13**, 102 (2018).
[53] J. M. Luttinger, Phys. Rev. **102**, 1030 (1956).
[54] N. R. Ogg, Proc. Phys. Soc. **89**, 431 (1966).
[55] U. Rössler, Solid State Commun. **49**, 943 (1984).
[56] P. Stano, C.-H. Hsu, M. Serina, L. C. Camenzind, D. M. Zumbühl, and D. Loss, Phys. Rev. B **98**, 195314 (2018).
[57] R. Winkler, *Spin-Orbit Coupling Effects in Two-Dimensional Electron and Hole Systems*, Springer Tracts in Modern Physics No. v. 191 (Springer, Berlin, New York, 2003).
[58] P. Pfeffer and W. Zawadzki, Phys. Rev. B **53**, 12813 (1996).
[59] We use $\gamma_1 = 4.285, \gamma_2 = 0.339, \gamma_3 = 1.446, \kappa = -0.42$, and $q = 0$ [57].
[60] Due to the relation $\mathbf{k} \times \mathbf{k} = -ie\mathbf{B}/\hbar$, the magnetic-field components are counted as quadratic in momentum.
[61] P.-O. Löwdin, J. Chem. Phys. **19**, 1396 (1951).
[62] An analogous set of terms for devices grown along [111] is given in the Supplemental Material.
[63] See Supplemental Material at http://link.aps.org/supplemental/10.1103/PhysRevLett.129.247701, which includes Refs. [64–75], for more details on the numerical values used in the calculation, and justification for the minimal model.
[64] S. Richard, F. Aniel, and G. Fishman, Phys. Rev. B **70**, 235204 (2004).
[65] T. Takahashi, T. Kodera, S. Oda, and K. Uchida, J. Appl. Phys. **109**, 034505 (2011).
[66] N. W. Hendrickx, D. P. Franke, A. Sammak, M. Kouwenhoven, D. Sabbagh, L. Yeoh, R. Li, M. L. V. Tagliaferri, M. Virgilio, G. Capellini, G. Scappucci, and M. Veldhorst, Nat. Commun. **9**, 2835 (2018).
[67] Y. Sun, S. E. Thompson, and T. Nishida, J. Appl. Phys. **101**, 104503 (2007).
[68] W. J. Hardy, C. T. Harris, Y.-H. Su, Y. Chuang, J. Moussa, L. N. Maurer, J.-Y. Li, T.-M. Lu, and D. R. Luhman, Nanotechnology **30**, 215202 (2019).
[69] S. Richard, F. Aniel, G. Fishman, and N. Cavassilas, J. Appl. Phys. **94**, 1795 (2003).
[70] Y. H. Huo, B. J. Witek, S. Kumar, J. R. Cardenas, J. X. Zhang, N. Akopian, R. Singh, E. Zallo, R. Grifone, D. Kriegner, R. Trotta, F. Ding, J. Stangl, V. Zwiller, G. Bester, A. Rastelli, and O. G. Schmidt, Nat. Phys. **10**, 46 (2014).
[71] M. Lodari, A. Tosato, D. Sabbagh, M. A. Schubert, G. Capellini, A. Sammak, M. Veldhorst, and G. Scappucci, Phys. Rev. B **100**, 041304(R) (2019).
[72] M. V. Fischetti, Z. Ren, P. M. Solomon, M. Yang, and K. Rim, J. Appl. Phys. **94**, 1079 (2003).
[73] A. V. Kuhlmann, J. Houel, A. Ludwig, L. Greuter, D. Reuter, A. D. Wieck, M. Poggio, and R. J. Warburton, Nat. Phys. **9**, 570 (2013).
[74] L. Kranz, S. K. Gorman, B. Thorgrimsson, Y. He, D. Keith, J. G. Keizer, and M. Y. Simmons, Adv. Mater. **32**, 2003361 (2020).
[75] G. Ithier, E. Collin, P. Joyez, P. J. Meeson, D. Vion, D. Esteve, F. Chiarello, A. Shnirman, Y. Makhlin, J. Schriefl, and G. Schön, Phys. Rev. B **72**, 134519 (2005).
[76] The limit is subtle, as it does not commute with evaluating matrix elements of differential operators (Appendix C in Ref. [77], Appendix B in [78]).
[77] M. J. Carballido, C. Kloeffel, D. M. Zumbühl, and D. Loss, Phys. Rev. B **103**, 195444 (2021).
[78] G. E. Simion and Y. B. Lyanda-Geller, Phys. Rev. B **90**, 195410 (2014).
[79] P. Stano, C.-H. Hsu, L. C. Camenzind, L. Yu, D. Zumbühl, and D. Loss, Phys. Rev. B **99**, 085308 (2019).
[80] G. Scappucci, C. Kloeffel, F. A. Zwanenburg, D. Loss, M. Myronov, J.-J. Zhang, S. De Franceschi, G. Katsaros, and M. Veldhorst, Nat. Rev. Mater. **6**, 926 (2021).
[81] C. Gradl, R. Winkler, M. Kempf, J. Holler, D. Schuh, D. Bougeard, A. Hernández-Mínguez, K. Biermann, P. V. Santos, C. Schüller, and T. Korn, Phys. Rev. X **8**, 021068 (2018).
[82] We have derived twelve terms which are fourth-order in momentum and first-order in electric fields. We examined

their influence on the dephasing and g factor for realistic parameters, and found them negligible.
[83] We thank Chen-Hsuan Hsu for clarifying this aspect for us [84].
[84] C.-H. Hsu, Electric field fluctuation due to various noise sources, Technical Report No. 2021-01-25, RIKEN, 2021.
[85] Including growth directions [011] or [111] instead of [001], harmonic or hard-wall confinement along the growth direction instead of the triangular one, and Ge or GaAs instead of Si. These data are not shown, except for a plot for Si grown along [111] with a triangular confinement, which is in the Supplemental Material.
[86] They are proportional to magnetic field; some of them are given in Eq. (2a). We found that such higher-order terms influence g-factor non-negligibly in n-GaAs in Ref. [56].
[87] D. Brunner, B. D. Gerardot, P. A. Dalgarno, G. Wüst, K. Karrai, N. G. Stoltz, P. M. Petroff, and R. J. Warburton, Science **325**, 70 (2009).
[88] For $1/f$ noise, the dephasing time under a Hahn-echo equals [75] T_2^* times $\sqrt{\ln(1/2\pi f_{\rm ir}t)/\ln 2}$, evaluating to 3.7 for the parameters given in the caption of Fig. 3.
[89] B. M. Freeman, J. S. Schoenfield, and H. Jiang, Appl. Phys. Lett. **108**, 253108 (2016).
[90] Using the hyperfine coupling coefficient for silicon in Ref. [91] with Eq. (29) of Ref. [92], we obtain $T_2^* = 6$ μs, while for purified silicon with 800 ppm we get $T_2^* = 0.3$ ms.
[91] P. Philippopoulos, S. Chesi, and W. A. Coish, Phys. Rev. B **101**, 115302 (2020).
[92] T. Struck, A. Hollmann, F. Schauer, O. Fedorets, A. Schmidbauer, K. Sawano, H. Riemann, N. V. Abrosimov, Ł. Cywiński, D. Bougeard, and L. R. Schreiber, npj Quantum Inf. **6**, 40 (2020).
[93] N. Piot, B. Brun, V. Schmitt, S. Zihlmann, V. P. Michal, A. Apra, J. C. Abadillo-Uriel, X. Jehl, B. Bertrand, H. Niebojewski, L. Hutin, M. Vinet, M. Urdampilleta, T. Meunier, Y.-M. Niquet, R. Maurand, and S. D. Franceschi, Nat. Nanotechnol. **17**, 1072 (2022).